Available online at www.sciencedirect.com
ScienceDirect
International Journal of Heat and Mass Transfer 51 (2008) 4480–4495
International Journal of HEAT and MASS TRANSFER
www.elsevier.com/locate/ijhmt

Experimental study and theoretical analysis of local heat transfer distribution between smooth flat surface and impinging air jet from a circular straight pipe nozzle

Vadiraj Katti, S.V. Prabhu *

Department of Mechanical Engineering, Indian Institute of Technology, Bombay, Powai, Mumbai 400 076, India

Received 22 March 2007; received in revised form 23 August 2007
Available online 24 March 2008

Abstract

An experimental investigation is performed to study the effect of jet-to-plate spacing and Reynolds number on the local heat transfer distribution to normally impinging submerged circular air jet on a smooth and flat surface. A single jet from a straight circular nozzle of length-to-diameter ratio (l/d) of 83 is tested. Reynolds number based on nozzle exit condition is varied between 12,000 and 28,000 and jet-to-plate spacing between 0.5 and 8 nozzle diameters. The local heat transfer characteristics are estimated using thermal images obtained by infrared thermal imaging technique. Measurements for the static wall pressure distribution due to impinging jet at different jet-to-plate spacing are made. The local heat transfer distributions are analyzed based on theoretical predictions and experimental results of the fluid flow characteristics in the various regions of jet impingement. The heat transfer at the stagnation point is analyzed from the static wall pressure distribution. Semi-analytical solution for heat transfer in the stagnation region is obtained assuming an axisymmetric laminar boundary layer with favourable pressure gradient. The heat transfer in the wall jet region is studied considering fluid flow over a flat plate of constant heat flux. However, heat transfers in the transition region are explained from reported fluid dynamic behaviour in this region. Correlations for the local Nusselt numbers in different regions are obtained and compared with experimental results.

Keywords: Single circular jet; Jet impingement; Forced convection; Heat transfer enhancement

1. Introduction

Impinging jets have received considerable attention due to their inherent characteristics of high rates of heat transfer. Such impinging flow devices allow for short flow paths and relatively high rates of cooling from comparatively small surface area. Various industrial processes involving high heat transfer rates use impinging jets. Few industrial processes which employ impinging jets are drying of food products, textiles, films and papers, processing of some metals and glass, cooling of gas turbine blades and outer wall of the combustion chamber, cooling of electronic equipments, etc. Heat transfer rates in case of impinging jets are influenced by various parameters like Reynolds number, jet-to-plate spacing, radial distance from stagnation point, Prandtl number, target plate inclination, confinement of the jet, nozzle geometry, curvature of target plate, roughness of the target plate and turbulence intensity at the nozzle exit.

Many prior studies are mostly on jet impinging over flat and smooth surface. Review of the experimental work on heat transfer to impinging jets is reported by Livingood and Hrycak [1], Martin [2], Jambunathan et al. [3] and Viskanta [4]. Gardon and Cobonpue [5] reported the heat transfer distribution between circular jet and flat plate for the nozzle plate spacing greater than two times the diameter of jet, both for single jet and array of jets. Specially

* Corresponding author. Tel.: +91 22 25767515; fax: +91 22 25726875/3480.
E-mail addresses: svprabhu@me.iitb.ac.in, svprabhu@iitb.ac.in (S.V. Prabhu).

0017-9310/$ - see front matter © 2008 Elsevier Ltd. All rights reserved.
doi:10.1016/j.ijheatmasstransfer.2007.12.024

Nomenclature

A	surface area for smooth surface (m^2)
a_1	constant in Eq. (9)
b_1	constant in Eq. (9)
d	diameter of the nozzle exit (m)
D	diameter of the air leading pipe (m)
E	enhancement factor defined in Eq. (17)
h	heat transfer coefficient (W/m^2 K)
h_0	heat transfer coefficient at the stagnation point (W/m^2 K)
I	current (A)
k	thermal conductivity of air (W/m K)
l	length of the nozzle pipe (m)
Nu	Nusselt number (hd/k)
Nu_0	stagnation Nusselt number (hd/k)
P	absolute wall static pressure (Pa)
P_0	absolute wall static pressure at stagnation point (Pa)
Δp	static wall pressure at any radius from stagnation (Pa)
Δp_0	static wall pressure at stagnation point (Pa)
Pr	Prandtl number (ν/α)
q	Heat flux (W/m^2)
q_{conv}	net heat flux convected to the impinging jet (W/m^2)
q_{joule}	imposed Ohmic heat flux, (VI/A) (W/m^2)
q_{loss}	total heat flux loss from impingement plate (W/m^2)
$q_{rad(f)}$	radiation heat loss from the front surface of impingement plate (W/m^2)
$q_{rad(b)}$	radiation heat loss from the back surface of impingement plate (W/m^2)
q_{nat}	heat loss by natural convection from the back surface of impingement plate (W/m^2)
$\overline{R}$	characteristic gas constant of jet fluid (kJ/kg K)
r	radial distance from the stagnation point (m)
Re	Reynolds number ($\rho\overline{V}d/\mu$)
T_j	jet air temperature (°C)
T_r	temperature of the target plate at given radial location (°C)
T_0	fluid temperature at the stagnation point (K)
U_m	maximum local radial velocity on target plate (m/s)
V	voltage (V)
$\overline{V}$	average velocity of flow at nozzle exit (m/s)
x	distance from leading edge of flat plate (m)
z	nozzle plate spacing (m)

Greek symbols

α	thermal diffusivity of jet fluid (m^2/s)
δ	characteristic length of radial wall jet boundary layer
δ_m	height of maximum radial velocity above target surface
μ	viscosity of air (Pa s)
ν	kinematic viscosity of jet fluid (m^2/s)
π_m	turbulence kinetic energy
ρ	density of air corresponding to supply pressure (kg/m^3)

designed heat flux gage were used for the measurement of local heat transfer distribution from a constant wall temperature plate. Gardon and Akfirat [6] studied the effect of turbulence on the heat transfer between two-dimensional jet and flat plate. Gardon and Akfirat [7] studied effect of multiple two-dimensional jets on the heat transfer distribution. Baughn and Shimizu [8] and Hrycak [9] conducted experiments of heat transfer to round jet from flat plate employing different methods of surface temperature measurement. Lytle and Webb [10] studied the effect of very low nozzle-to-plate spacing ($z/d < 1$) on the local heat transfer distribution on a flat plate impinged by a circular air jet issued by long pipe nozzle which allows for fully developed flow at the nozzle exit and found that in the acceleration range of the nozzle plate spacing ($z/d < 0.25$), maximum Nusselt number shifts from the stagnation point to the point of secondary peak and the effect being more pronounced at higher Reynolds number. Lee et al. [11] studied the effect of nozzle diameter on impinging jet heat transfer and fluid flow. They reported that local Nusselt numbers in the region corresponding to $0 \leqslant r/d \leqslant 0.5$ increased with increasing nozzle diameter. Beitelmal et al. [12] analyzed two-dimensional impinging jets and correlated heat transfers in the stagnation point, stagnation region and wall jet region with approximate solutions developed using simplified flow assumptions. Lienhard [13] analyzed heat transfer by impingement of circular free-surface liquid jets and analytical solutions were explained for heat transfer in different regions on the target plate.

Many prior studies were focused on the role of nozzle configuration on impingement heat transfer. Garimella et al. [14] conducted series of experiments to study the effect of nozzle length to diameter ratio on impingement heat transfer rates to confined submerged liquid jet of FC-77. They reported that square edged orifice of l/d less than 0.5 provide better heat transfer characteristics when compared with larger l/d. Lee and Lee [15] studied the effect of nozzle configuration for l/d of 0.2 with three different types of profiles at nozzle exit, i.e., square edged, standard edged and sharp edged orifices. The tests were carried out for unconfined air jets impinging normally on smooth flat surface and the heat transfer results show that at stagnation region sharp edged orifice performs better. Brignoni

and Garimella [16] studied the effect of nozzle inlet chamfering on pressure drop and heat transfer characteristics in confined air jet impingement choosing nozzle length to diameter ratio of 1.0. They concluded that chamfering the nozzle inlets reduce pressure drops without affecting much the heat transfer characteristics.

It is known that fluid flow behaviour over a heated surface dictates convective heat transfer characteristics. Flow of fluid over a surface due to an axisymmetric circular submerged jet impingement is complex in nature unlike flow over a flat plate. Most of the correlations proposed are for average heat transfer coefficients as reported by Zukerman and Lior [17]. Few correlations for stagnation point Nusselt numbers available are based on regression analysis from experimental data. There are contrasting opinions on the local heat transfer distribution reported by Gardon and Cobonpue [5], but no correlations are proposed. Hence, it is felt from the available literature that there is a need to obtain radial local distribution of heat transfer coefficients and generalized correlations for local heat transfer coefficients based on the flow characteristics on the target plate due to circular submerged jet impingement and the available semi-empirical predictions. Hence, the aim of the present paper is to

(a) conduct experimental investigations for local distribution of heat transfer coefficients and wall static pressure;
(b) analyze theoretically the local heat transfer characteristics due to axisymmetric submerged jet impingement; and
(c) obtain semi-empirical correlations for local heat transfer coefficients and compare the results with the experimental data.

2. Experimental set-up

The experimental set up layout is shown in Fig. 1. Air is supplied by an air compressor through a calibrated orifice flow meter. Air filter and pressure regulator are installed upstream of the orifice flow meter to filter the air and to maintain the downstream pressure at 4 bar. The flow rate is controlled by two needle valves, one on each side of the orifice flow meter. The function of the upstream needle valve is not to allow cooling air to flow until the compressor has built up the pressure in its reservoir above 4 bar. Actual flow rate is controlled by the downstream needle valve. The nozzle is an aluminum pipe of inner diameter of 7.35 mm and length to diameter ratio of 83, which is similar to that used by Lyttle and Webb [10]. This length ensures fully developed flow over the Reynolds number range investigated.

The target plate (80 mm × 160 mm; 0.06 mm thick stainless steel foil) is clamped tightly and stretched between two copper bus bars. Approximately 5 mm of the foil on either side is sandwiched in the bus bars to ensure firm grip. The target plate assembly is as shown in Fig. 2a. Because of the thinness of foil, lateral conduction is negligible and surface provides constant heat flux situation as reported by Lytle and Webb [10]. Thermal images are obtained from *IR* camera positioned on the side of the heater opposite the impinging nozzle. One dimensional energy balance across the heated plate shows negligible temperature difference across it. Hence, the local temperature measured on the back surface is considered to be same as that on the impingement plane. The back surface of heater element is painted black using a thin coat of 'Matt finish Asian' paint which provides high emissivity (0.99) surface. Infrared radiometry technique is used to measure local temperature

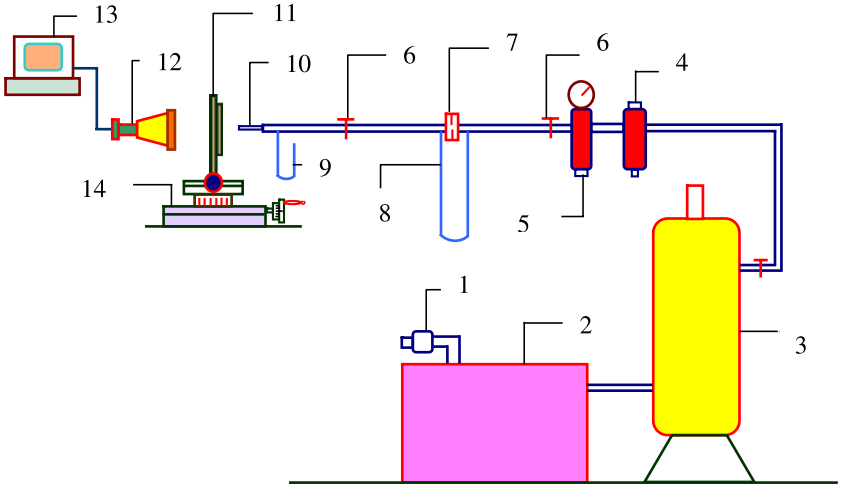

1) Air filter. 2) Air compressor. 3) Air receiver. 4) Air filter. 5) Pressure regulator. 6) Needle valves. 7) Orifice plate. 8) Differential manometer. 9) Simple manometer. 10) Nozzle. 11) Impingement plate assembly. 12) Infra red camera. 13) Computer. 14) Traverse system.

Fig. 1. Layout of experimental set-up.

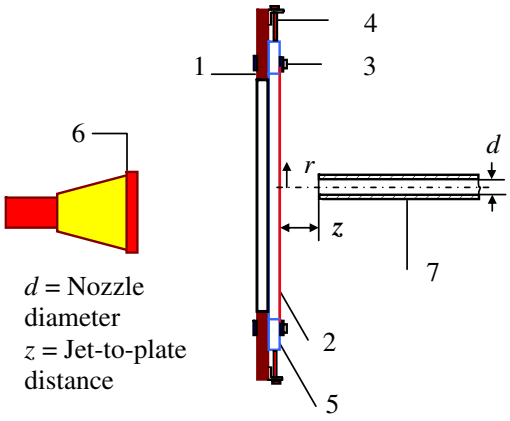

1). Frame. 2) Stainless steel foil. 3) Clamping screw 4) Stretching screw. 5) Copper bus bar. 6) I.R.Camera.7) Long-tube nozzle

Fig. 2a. Target plate assembly for heat transfer distribution.

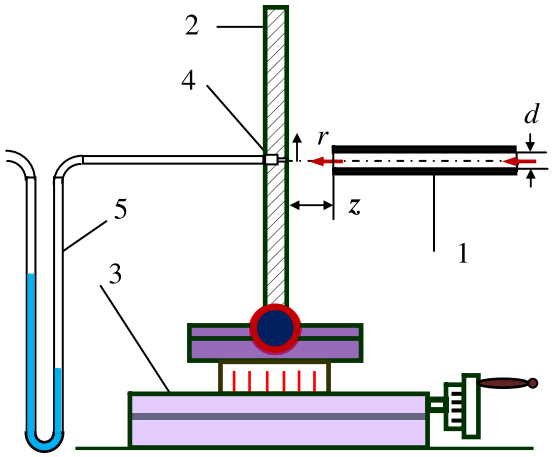

1) Long-tube nozzle 2) Acrylic target plate 3) Traversing table 4) Static wall pressure tap 5) U-Tube manometer

Fig. 2b. Target plate assembly for static wall pressure distribution.

from uniform heat flux surface which provides higher spatial resolution of temperature than thermocouples. 'Thermoteknix' Ti200 infrared camera is used to collect the local temperature distribution with a resolution of about 0.3 mm per pixel. Power is supplied from AC power source through a voltage stabilizer, a variac and a current transformer. The voltage across the heater and the current are measured by 'Meco' digital meters whose ranges and the accuracies are of 0 to $20 \pm 0.5\%$ V and 0 to $400 \pm 0.5\%$ A, respectively. Suitable voltage taps are provided in each of the bus bars. Jet air temperature is measured using a Chromel–Alumel thermocouple (K-type) positioned at the inlet of the nozzle. The output of the thermocouple is measured by 'Meco' millivoltmeter. A traverse system is used to set different jet-to-plate distances.

Thermal infrared camera reads the temperature of the plate depending on the emissivity value of the surface of the plate. Therefore, it is necessary to calibrate the emissivity of the surface. This is done by constructing a 100 mm size cubical tank from the same material as that of the target plate (i.e., stainless steel). This tank is painted with 'Matte Finish Asian' black paint to achieve uniform emissivity all over the surface. The tank is insulated from the five sides and one side is opened to the atmosphere. Tank is filled with water and is heated with a 500 W heater. A small motor driven stirrer is immersed in the water to maintain uniform temperature of the water bath. Two calibrated thermocouples are mounted on the exposed surface of the tank at two different locations. Initially, water in the tank is heated to the temperature of about 70 °C. Then, the heater is switched off and the temperature of the surface is allowed to decrease. The time constant of the temperature drop is about 3 min per 0.24 °C. This time is sufficient to obtain thermal images of the surface from the infrared camera and to note the thermocouple readings. The emissivity input to the images is then adjusted till the temperature read by the image is the same as that read by the thermocouples. This procedure is repeated for different temperatures of the exposed surface till it reached 35 °C. The average emissivity is found to be 0.99. The uncertainty in the temperature measurement is not more than ±0.5 °C.

Power loss from the exposed surface of the target plate due to natural convection and radiation is estimated experimentally. The corrections are included in calculation of local heat transfer coefficient.

Local wall pressure measurements are made on the same setup by replacing the stainless steel foil target plate with an acrylic plate as shown in Fig. 2b. A static pressure tap, approximately 0.5 mm in diameter, is drilled in 10 mm thick acrylic plate for 3 mm deep from impingement surface and then counterbored to 3 mm diameter for the remaining depth. This pressure tap is connected to U-tube water manometer. The traversing table is moved perpendicular to the nozzle axis to note radial distribution of static wall pressure.

3. Data reduction

The temperature distribution on the target plate is obtained by averaging ten thermal images for each configuration. Digitization of thermal images for radial temperature distribution on impingement surface is carried out in MATLAB. The Nusselt number for the smooth surface is calculated by

$$Nu = \frac{hd}{k} \tag{1}$$

$$h = \frac{q_{\text{conv}}}{T_r - T_j} \tag{2}$$

Heat transfer rate between impinging jet and target plate, q_{conv}, is estimated as follows:

$$q_{conv} = q_{joule} - q_{loss} \quad (3)$$

$$q_{loss} = q_{rad(f)} + q_{rad(b)} + q_{nat} \quad (4)$$

$$q_{joule} = \frac{VI}{A} \quad (5)$$

$$q_{loss} = q_{rad(f)} + q_{rad(b)} + q_{nat} = \text{Estimated experimentally} \quad (6)$$

Uncertainties in the measurement of heat transfer coefficients are carried out using the method suggested by Moffat [18] and are around 3.4% and 2.9%, respectively, at Reynolds number of 12,000 and 28,000.

4. Results and discussion

4.1. Comparison of the present results with those published in the literature

In the present study, the experimental setup and the nozzle is similar to those of Lytle and Webb [10]. Fig. 3 shows that stagnation point Nusselt numbers of the present study are in good agreement (within 4.8%) with the correlations for low z/d (less than 1.0) of Lytle and Webb [10]. The local Nusselt number at a given Reynolds number of 23,000 and z/d of 6 is compared with those of the earlier published data as shown in Fig. 4. It compares well with the results of Lytle and Webb [10] and Gao et al. [19].

4.2. Local heat transfer distribution

Local heat transfer distribution is measured for different jet to plate spacings (z/d) of 0.5, 0.75, 1.0, 2.0, 3.0, 4.0, 6.0 and 8.0 at Reynolds numbers of 12,000, 16,000, 20,000, 23,000 and 28,000. Fig. 5 shows the variation of Nusselt numbers at the stagnation point for all z/ds covered in the study at a Reynolds number of 23,000. It is observed that stagnation point Nusselt numbers increase with z/d from $z/d = 1.0$ up to around $z/d = 6.0$ and then slightly drop. This trend may be due to increase in turbulent inten-

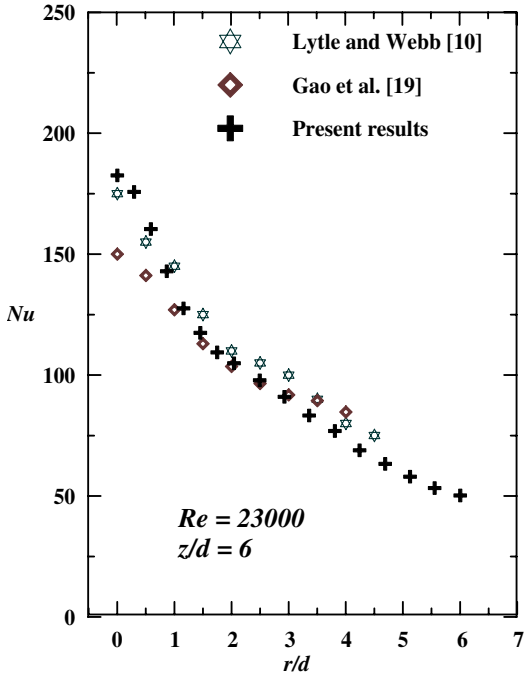

Fig. 4. Comparison of results with previous researchers for Nusselt number distribution.

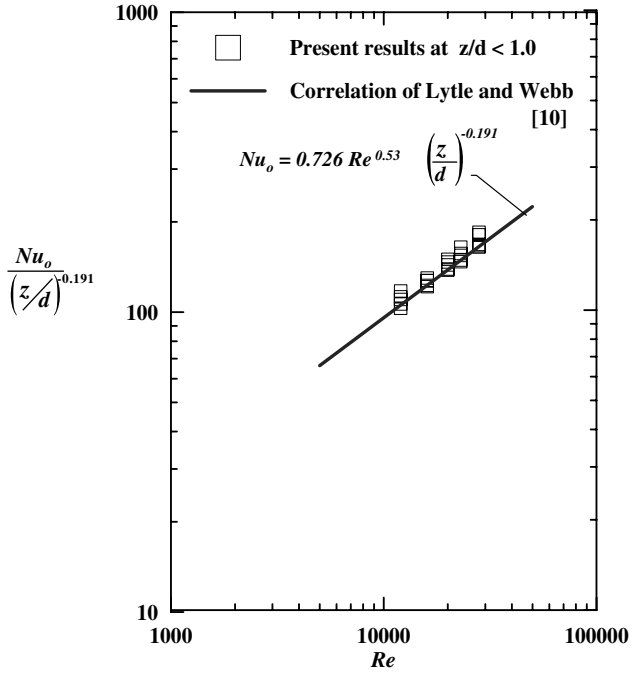

Fig. 3. Comparison of stagnation point Nusselt numbers with the correlation of Lytle and Webb [10].

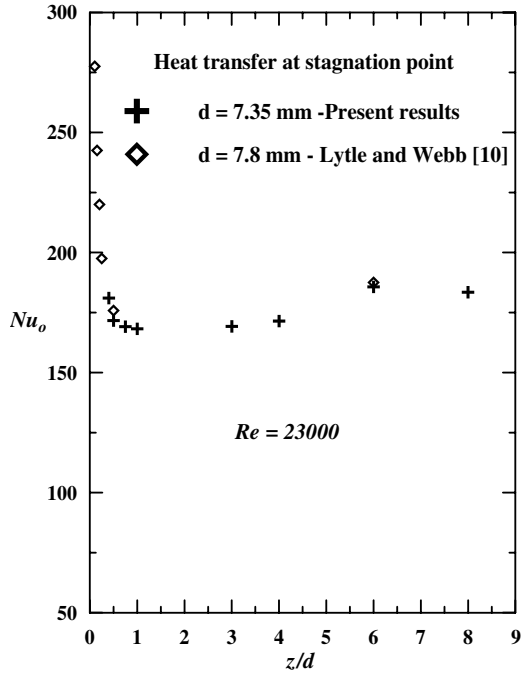

Fig. 5. Effect of jet-to-plate distance on the heat transfer at the stagnation point.

sity at the stagnation point with increase in z/d. The experimental results of Cooper et al. [20] show the dependence of the stagnation Nusselt number for $z/d \geqslant 2.0$ with near wall axial turbulent intensities. At $z/d = 2.0$, near wall axial turbulent intensities are around 5%. However, at $z/d = 4.0$ and 6.0, near wall axial turbulent intensities are around 12.8%. Higher near wall axial turbulence intensity at larger jet-to-plate distances has been attributed to the spreading of the mixing layer that originates from the rim of the nozzle to the jet axis. Fig. 5 shows that the stagnation point Nusselt numbers of the present study compare well with those of Lytle and Webb [10].

Fig. 6 shows the distribution of local Nusselt number on the surface at $Re = 28{,}000$ for $z/d = 0.5$, 1.0, 4.0 and 8.0. The secondary peaks are observed for $z/d = 0.5$ and 1.0 whereas, Nusselt numbers attenuate monotonically for $z/d = 4.0$ and 8.0. The profiles of the local Nusselt number distribution are estimated by performing circumferential average at each radial location from the stagnation point.

Figs. 7 and 8 show local distribution of Nusselt numbers for z/ds from 0.5 to 8.0 for five jet Reynolds numbers from 12,000 to 28,000. The heat transfer coefficients increase with increase in Reynolds number at all radial locations. The stagnation point Nusselt number is highest for a given Reynolds number. For z/ds lower than 3.0 and Reynolds numbers of 20,000, 23,000 and 28,000, Nusselt numbers decrease from the stagnation point and reach a local minimum at an r/d of about 1.0 to 1.2 and then increase to form a secondary peak. Further in the downstream, Nusselt numbers decay monotonically. However, secondary peaks are not distinctly seen for lower Reynolds numbers of 12,000 and 16,000. Increase in the Nusselt numbers at the secondary peak from the local minimum is higher for $z/d = 0.5$ and Reynolds number of 28,000 (about 9%)

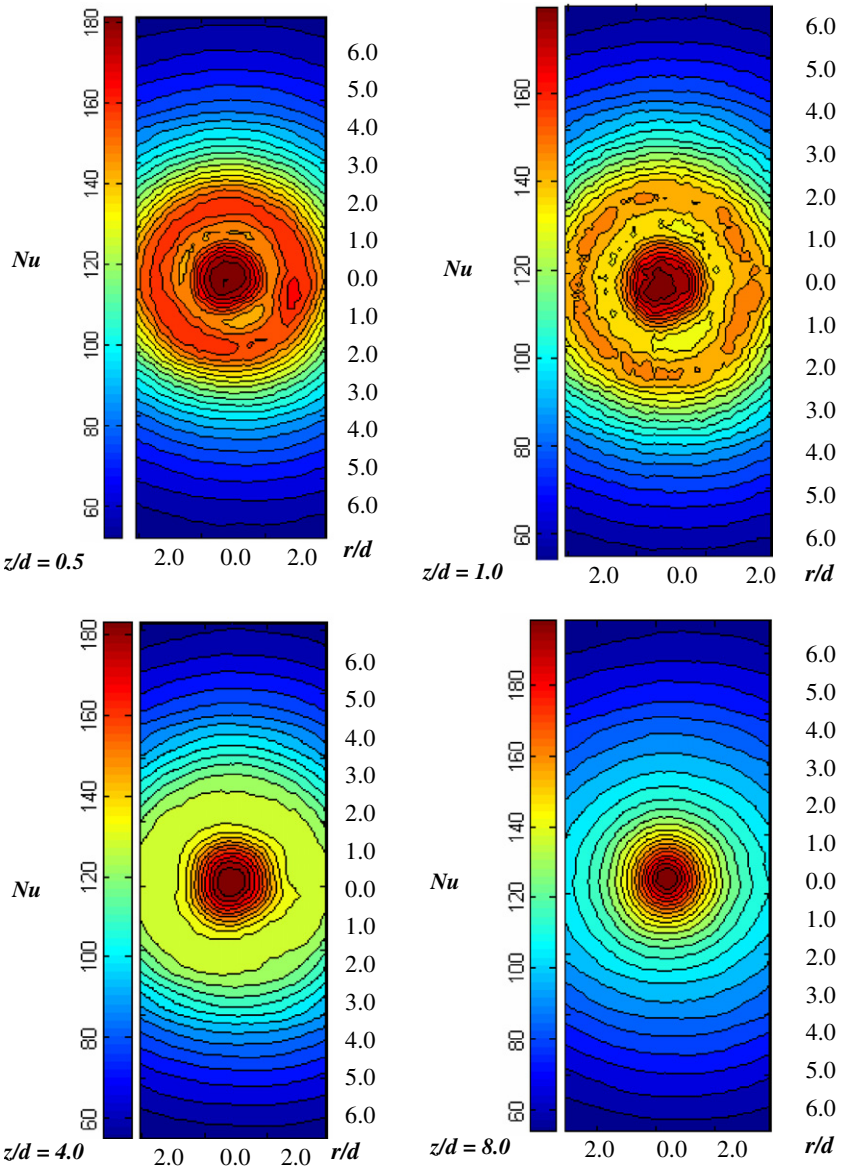

Fig. 6. Distribution of local Nusselt number at $Re = 28{,}000$ for $z/d = 0.5$, 1.0, 4.0 and 8.0.

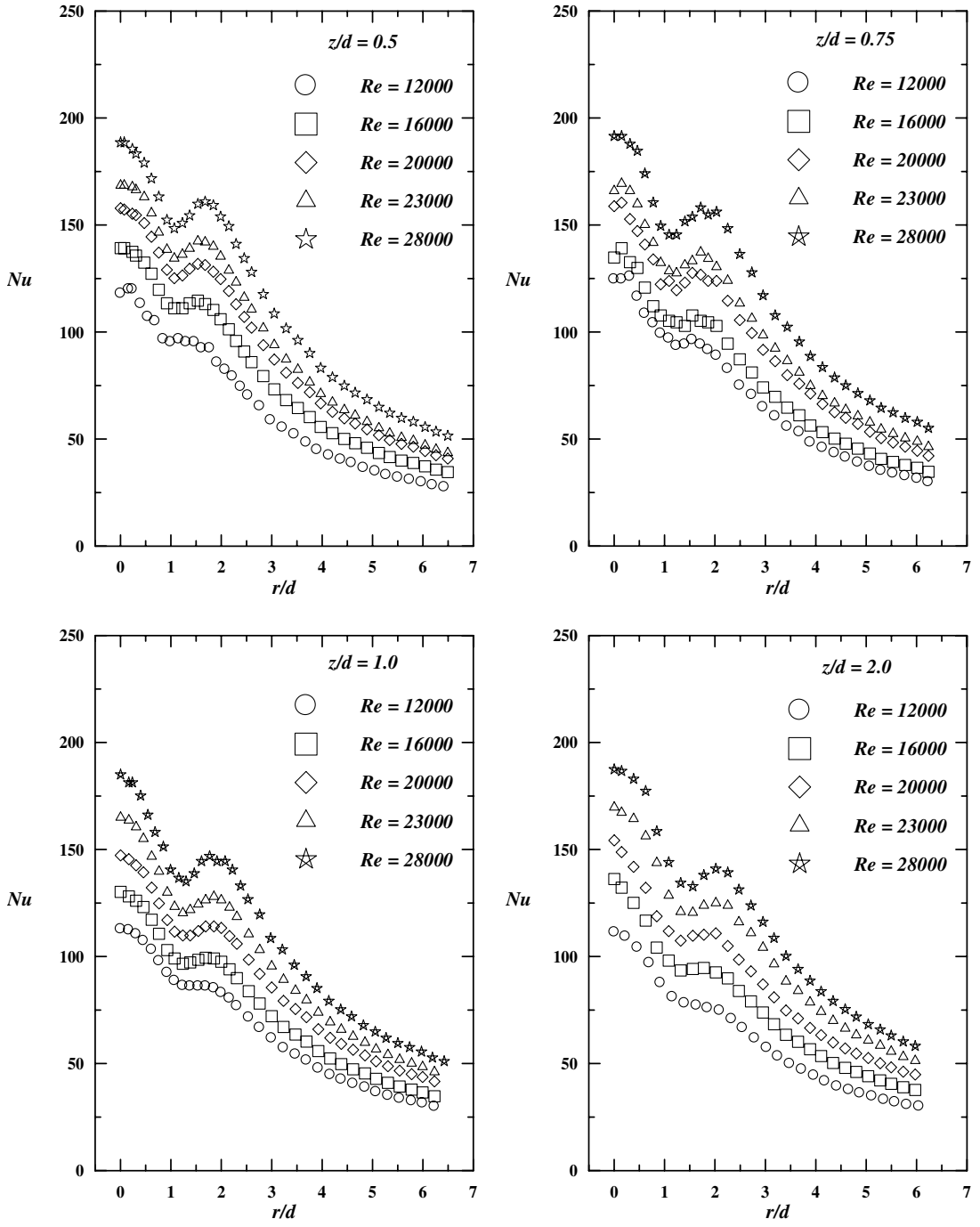

Fig. 7. Local heat transfer distribution for normal impingement of jet from a long pipe nozzle on a smooth surface.

and occurs at an r/d of about 1.70. However, secondary peaks are less pronounced with higher z/d. The location of secondary peaks shifts slightly towards the stagnation point with decrease in the Reynolds number. It is observed that radial location of secondary peak shifts away from the stagnation point as z/d is increased from 0.5 to 3.0. These observations are supported by the measurements of near-wall RMS velocity fluctuations in the radial direction by Lytle and Webb [10] for lower z/ds. Thus, Nusselt numbers at the secondary peak is due to significantly higher turbulence in the boundary layer resulting from intense shear between the radially exiting wall-jet and the stagnant surrounding as z/d decreases. It can be further contemplated that, the fluid accelerations and stronger shear interaction with surrounding may promote an increase in turbulence at lower r/d for smaller jet-to-plate spacing. At $z/d = 3.0$, secondary peak occurs at r/d of about 2.0. At $z/d = 4.0$, secondary peak almost vanishes but sharp decrease in the slope of distribution of local Nusselt numbers are seen at an r/d of about 1.2 and increase in the slope at r/d of 2.2.

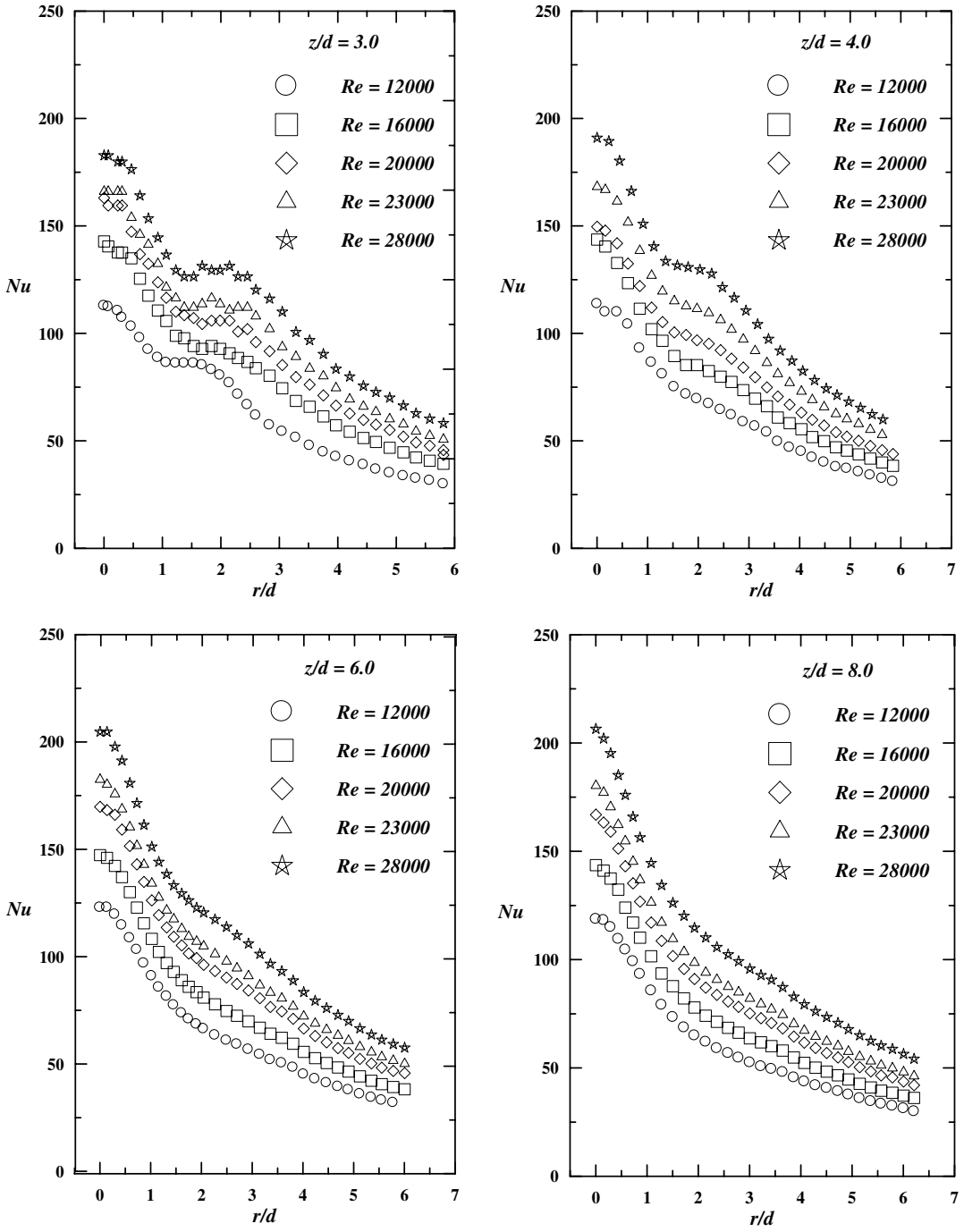

Fig. 8. Local heat transfer distribution for normal impingement of jet from a long pipe nozzle on a smooth surface.

For all Reynolds numbers, it is seen that the heat transfer coefficients decrease monotonically in the radial direction away from the stagnation point for z/d of 6.0 and 8.0. Instead of secondary peak, a mild decrease in the slope of distribution of local Nusselt numbers can be observed at an r/d of about 1.5.

Heat transfer characteristics due to jet impingement can be better understood if the regions on the target plate are suitably identified. The center line velocity of the impinging jet is highest and reduces to zero at the point of impact on the flat target surface, i.e., the stagnation point. At the stagnation point, the wall static pressure is highest and higher than the atmospheric pressure. This results in a favourable pressure gradient along a direction parallel to the target surface in the stagnation region. Finally, the flow over the target surface forms the wall jet region. The wall jet adheres to the surface and flows over the plate interacting with the surrounding air. Fig. 9 shows the present experimental results of heat transfer and wall static pressure distribution on the target surface for $z/d = 0.5$ and

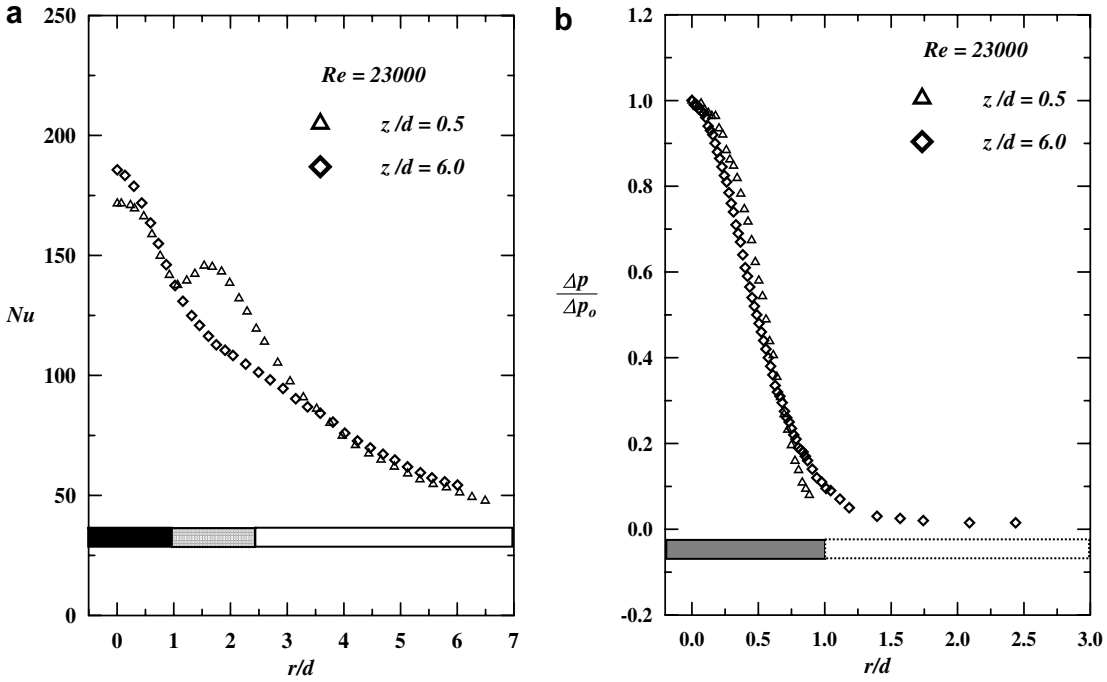

Fig. 9. Identification of regions based on local heat transfer and wall static pressure distribution over the target surface due to circular jet impingement.

6.0 at Reynolds number of 23,000. The heat transfer distribution pattern shows three distinct regions and they are represented by three shade bands. These three regions on the target surface with axisymmetric circular jet impingement are shown schematically in Fig. 10.

4.3. Analysis of local distribution of heat transfer characteristics

4.3.1. Heat transfer rates at the stagnation point ($r/d = 0$)

Heat transfer rates at stagnation point can be analyzed based on wall static pressure distribution data. Theoretical solution for heat transfer coefficient at the stagnation point in case of laminar jet of an infinite extent impinging normally on a flat surface is given by Burmeister [21]

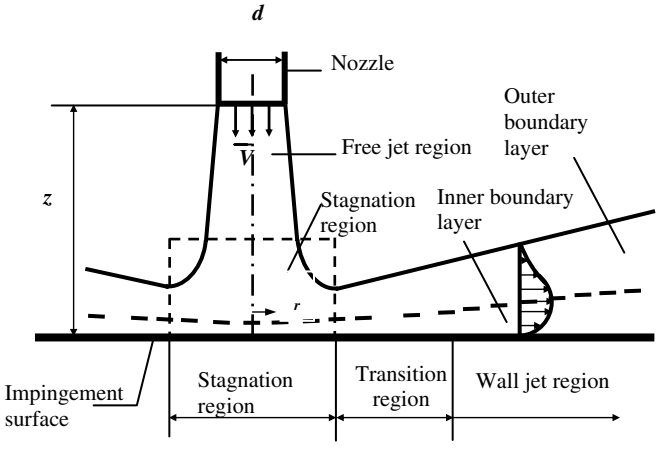

Fig. 10. Regions on the target surface due to an impinging circular jet.

$$h_0 = 0.44k(3^{0.5})\left(\frac{C}{v}\right)^{0.5} \tag{7}$$

The constant C in Eq. (7) can be considered as velocity gradient at the stagnation point of finite jet. According to Gauntner et al. [22], the local radial velocity gradient at the stagnation is a parameter influencing stagnation point heat transfer coefficients. The local radial velocity gradient at the stagnation point from static wall pressure distribution in the vicinity of stagnation point, assuming incompressible flow can be expressed as in Eq. (8)

$$\left(\frac{\mathrm{d}U_{\mathrm{m}}}{\mathrm{d}r}\right)_{r=0} = \sqrt{\left(\frac{2\overline{R}}{R^2}\right)}\sqrt{\frac{T_s\left(1-\frac{P}{P_0}\right)}{\left(\frac{r}{R}\right)^2}} \tag{8}$$

The static wall pressure data in the form $(1 - P/P_0)$ are drawn as a function of $(r/R)^2$and slope of the resulting curve at the stagnation point ($r = 0$) is evaluated graphically. A typical variation of these parameters for $z/d = 8.0$ and Reynolds number of 20,000 is shown in Fig. 11a. Substituting this in Eq. (8), radial velocity gradient at the stagnation point (C) can be computed. In the present experiments, local wall static pressures in the neighborhood of stagnation point are measured and for the configurations studied stagnation point Nusselt numbers are evaluated from the above Eqs. (7) and (8). Fig. 11b shows the estimated and present experimental values of the Nusselt numbers at the stagnation point at different jet-to-plate spacing. It is seen that experimental Nusselt numbers at the stagnation point are higher compared to those obtained by theoretical correlation. This may be attributed to the

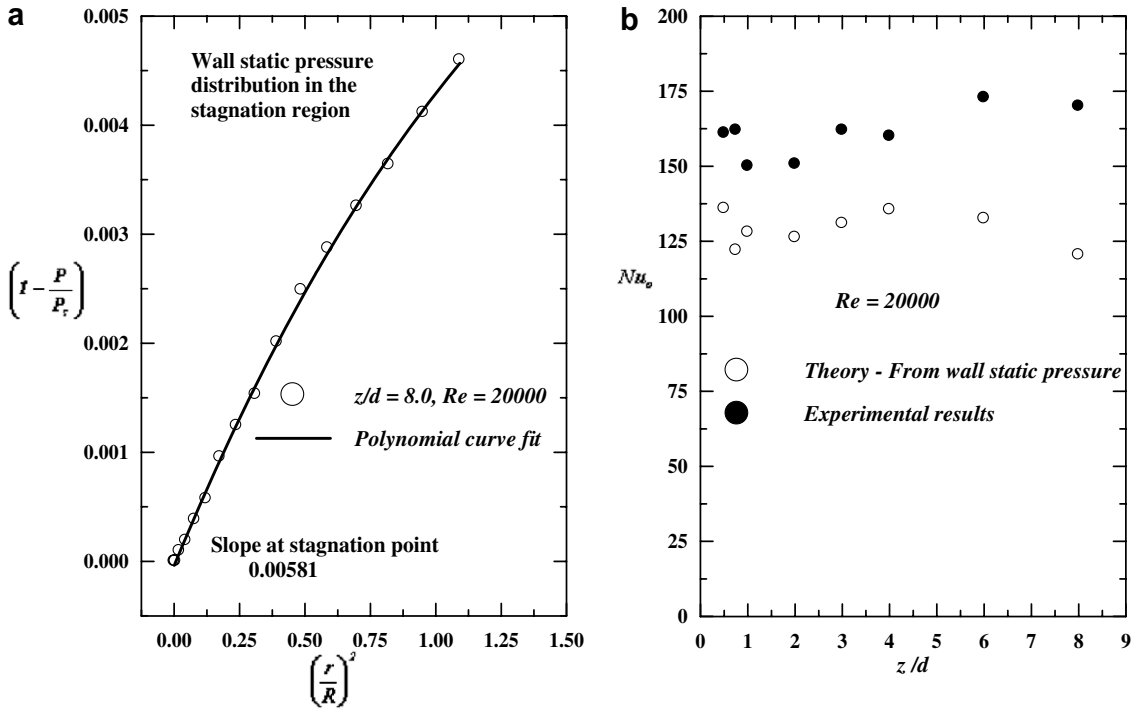

Fig. 11. (a) Estimation of velocity gradient from static wall pressure data. (b) Heat transfers at stagnation point and their comparison with that estimated from velocity gradient at stagnation point.

small turbulent intensities close to the stagnation point resulting in higher heat transfer coefficients. It is observed that the trend in the estimated values of Nusselt numbers at the stagnation point reasonably match with the experimental results.

4.3.2. Heat transfer rates in the stagnation region ($0 < r/d < 1.0$)

For the flow in the stagnation region, an analytical solution for an axisymmetric jet impinging normally on flat smooth surface assuming an axisymmetric laminar boundary layer with pressure gradient is presented by Brdlik and Savin [23]. An expression for local Nusselt number may be obtained and is modified to the form

$$\frac{Nu}{Re^{1/2}Pr^{1/3}} = a_1\left(\frac{z}{d}\right)^{-0.11}\left(1-\frac{\left(\frac{r}{d}\right)^2\left(\frac{z}{d}\right)^{-0.2}}{b_1}\right)^{1.2} \tag{9}$$

Brdlik and Savin [23] reported constant values for a_1 and b_1 for different jet-to-plate spacing. This may be true with their experimental setup which uses thick copper plate as heater surface. So, their data for heat transfer coefficient distribution is not truly local. But, present experimental results show the variation in the values of constants a_1 and b_1 with z/d and are detailed in Table 1. At $r/d = 0$, the above equation reduces to a case of Nusselt number at the stagnation point and is given by

$$Nu_0 = a_1 Re^{1/2}Pr^{1/3}(z/d)^{-0.11} \tag{10}$$

Table 1
Values of constants a_1 and b_1 for different z/d used in Eq. (9)

z/d	0.5	0.75	1.0	2.0	3.0	4.0	6.0	8.0
a_1	1.15	1.2	1.2	1.32	1.4	1.42	1.6	1.63
b_1	5.3	5.1	4.6	3.6	3.2	3.2	2.9	2.3

Fig. 12 shows the distribution of Nusselt numbers at the stagnation point for different z/d computed from Eq. (10) and compare well with the present experimental results within 6%. The comparison of the local heat transfer distribution at $z/d = 0.5$ obtained by modified Brdlik and Savin's correlation (Eq. (9)) and experimental results are shown in Fig. 13. It is observed that the local Nusselt numbers in the stagnation region estimated by modified Brdlik and Savin's correlation compare better with the experimental values within around ±6%. The results from present experiments and theoretical analysis show that the Nusselt numbers depend on distance from stagnation point in the stagnation region and heat transfer coefficients decrease from the stagnation point till the edge of stagnation region. This may be because of small increase in boundary layer thickness in the radial direction. However, Beitelmal et al. [12] in their analysis for heat transfer in the stagnation region report that Nusselt numbers in this region are independent of distance from stagnation point.

4.3.3. Heat transfer rates in transition region ($1.0 < r/d < 2.5$)

The flow from stagnation region to wall jet region occurs through the transition where the boundary layer

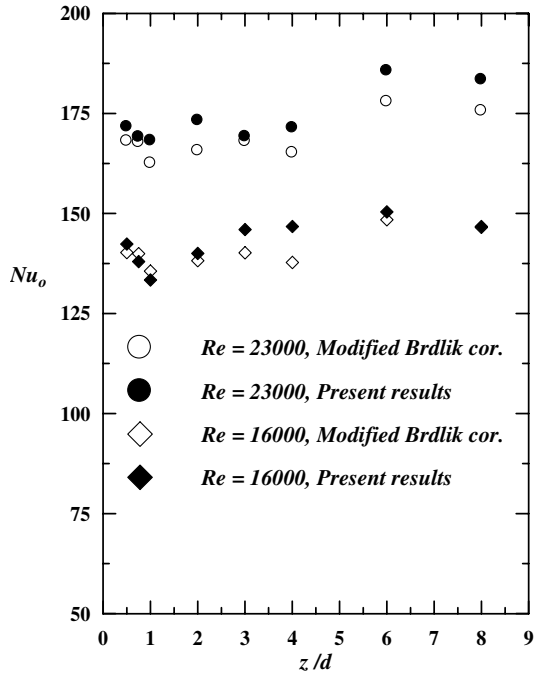

Fig. 12. Heat transfer at stagnation point and their comparison with modified Brdlik and Savin correlation.

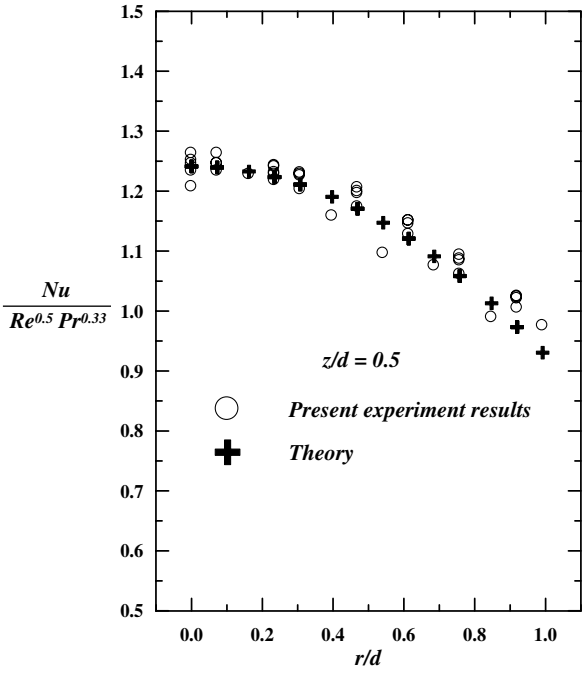

Fig. 13. Local heat transfer distribution in stagnation region and comparison with modified Brdlik and Savin correlations.

changes from laminar to turbulent. From the edge of the stagnation region ($r/d = 1.0$), transition region can be considered to extend up to an r/d of about 2.5. It is observed from Figs. 7–9a, that this region is sensitive to jet-to-plate distances.

Observations in the transition region may be explained from the fluid dynamic measurements reported by Knowles and Myszko [24]. Shear stress distribution along the wall in the radial direction for different z/d shows that shear stress sharply increases for lower z/d from r/d of about 1.0 and attains a peak at around r/d of about 2.0 and then drops. Fig. 14 shows radial distribution of peak production of

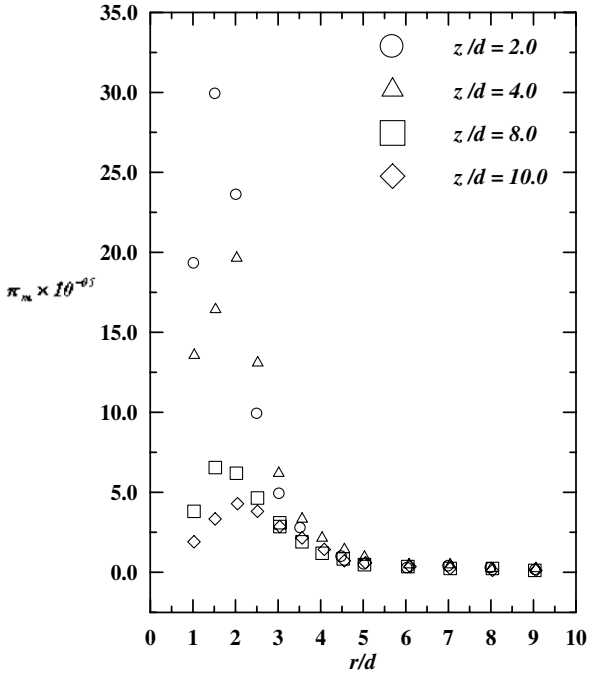

Fig. 14. Peak production of turbulent kinetic energy for different jet-to-plate spacing (reproduced from Knowles and Myszko [24]).

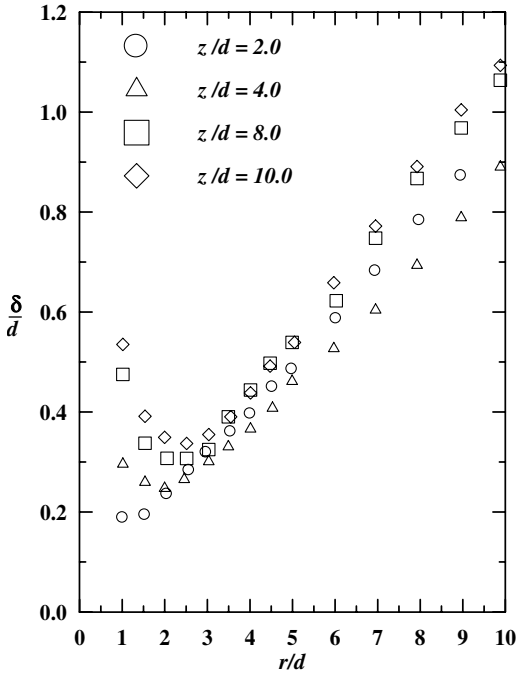

Fig. 15. Variation of wall jet growth rates with jet-to-plate spacing (reproduced from Knowles and Myszko [24]).

turbulent kinetic energy as reported by Knowles and Myszko [24]. It is observed that the turbulent intensities of the main jet and wall jet peak at r/d of about 2.0 and is highest for lowest z/d (= 2.0) investigated. This explains the occurrence and location of secondary peaks in heat transfer coefficients in the transition region for lower z/ds.

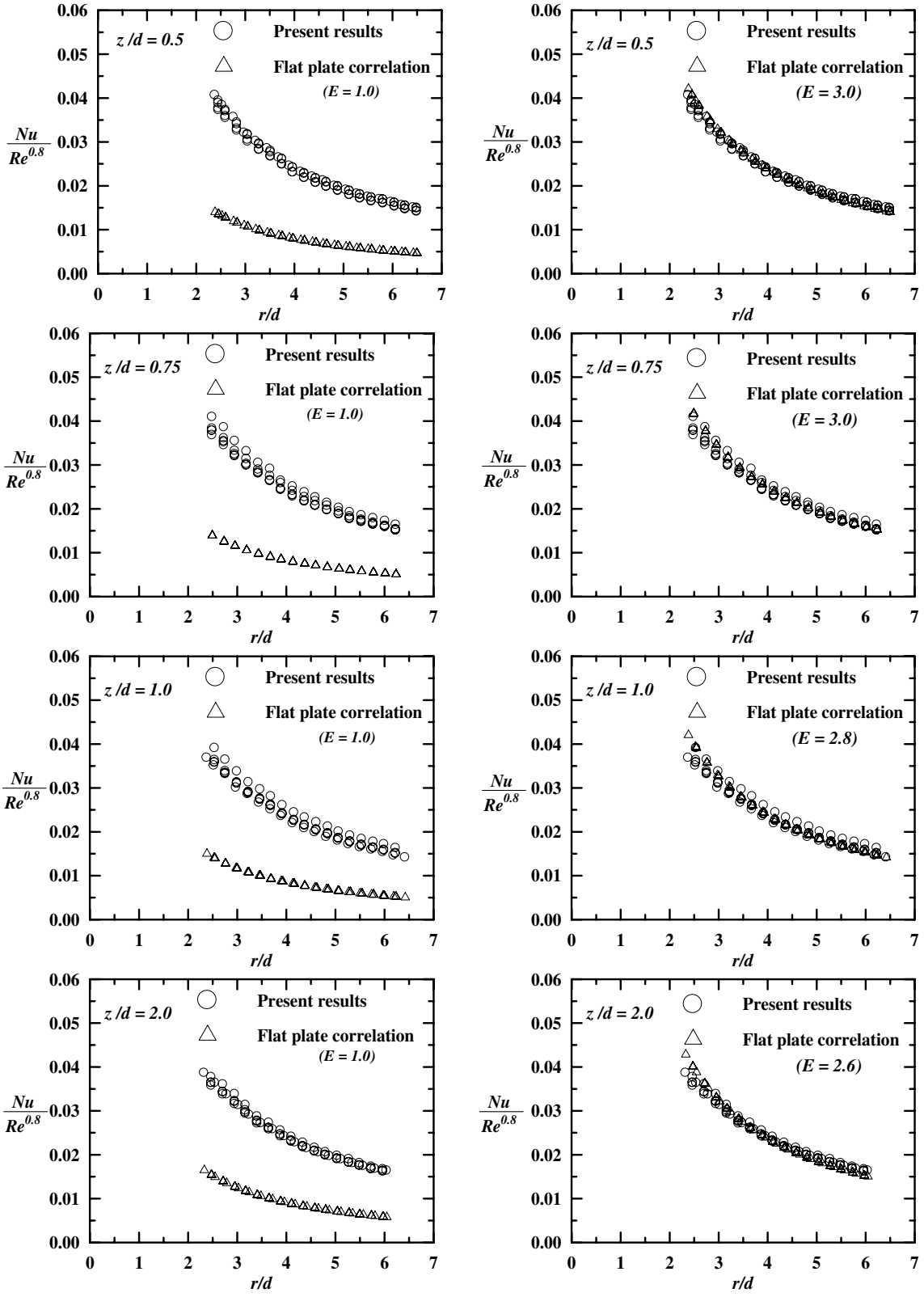

Fig. 16. Local heat transfer distribution in the wall jet region ($r/d > 2.5$) and comparison with theoretical correlations.

Fig. 15 shows typical growth rate of the boundary layer of the wall jet for different jet-to-plate spacing from the experiments of Knowles and Myszko [24]. The trends shown match with the results of Cooper et al. [20] and Poreh et al. [25]. It is observed that wall jet for all z/d grows linearly from a radial distance of about $2.5d$. Thus, it may be inferred that wall jet region commences from r/d of about 2.5 and region of transition extends from $r/d = 1.0$

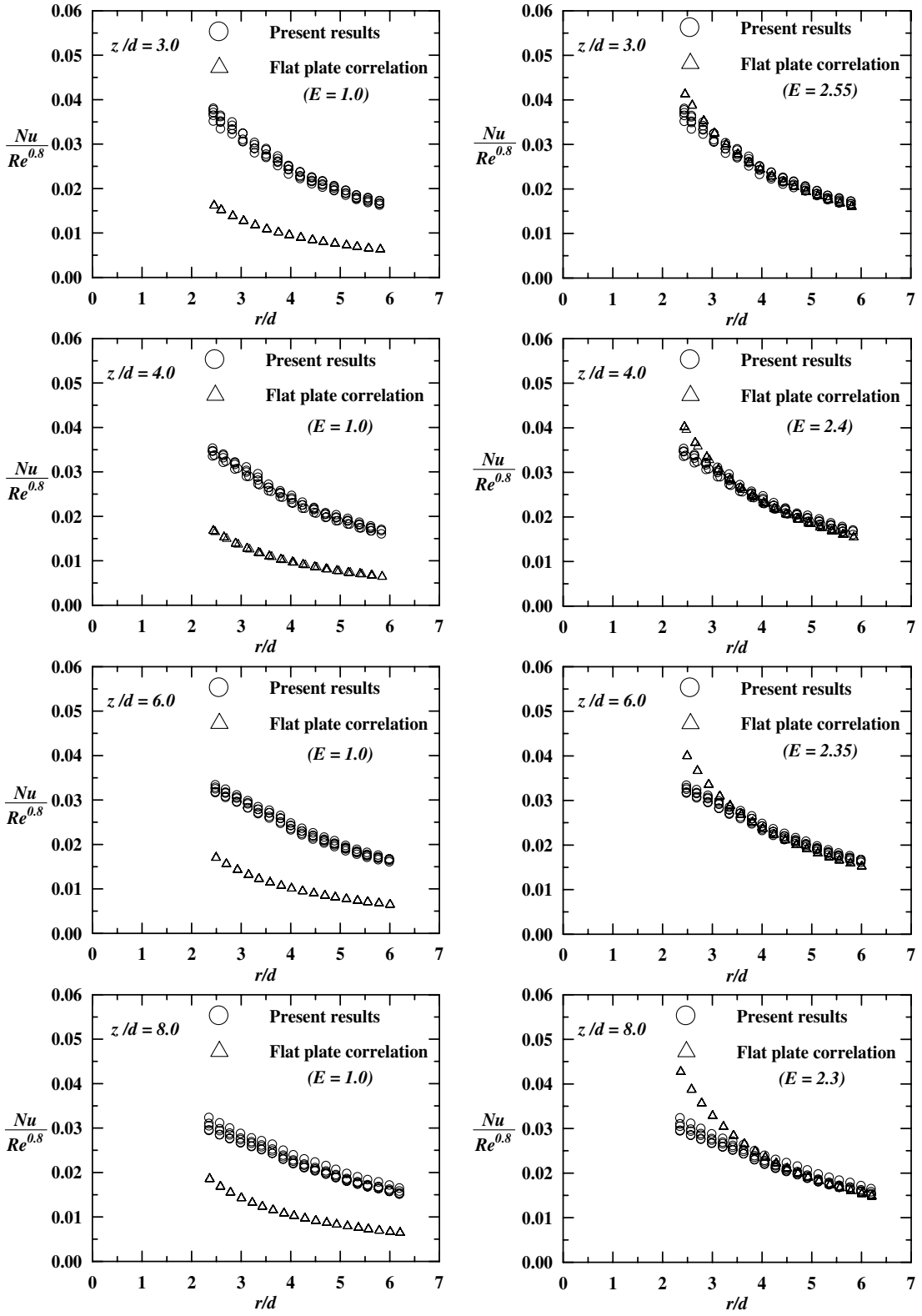

Fig. 17. Local heat transfer distribution in the wall jet region ($r/d > 2.5$) and comparison with theoretical correlations.

to 2.5. It is observed that characteristic boundary layer thickness of wall jet (δ/d) is thinner for lower z/d and hence the heat transfer coefficients in this region are higher.

Correlations are developed from the experimental data using least square fit separately for two ranges of jet-to-plate distances in the transition region and are as given below by Eqs. (11) and (12)

$$\text{For } z/d \leqslant 3.0 \quad Nu = 0.2636Re^{0.6188}\left(\frac{z}{d}\right)^{-0.0898}\left(\frac{r}{d}\right)^{-0.074} \tag{11}$$

$$\text{And for } z/d \geqslant 4.0 \quad Nu = 0.198Re^{0.6632}\left(\frac{z}{d}\right)^{-0.0826}\left(\frac{r}{d}\right)^{-0.3702} \tag{12}$$

Values estimated from the above correlations compare with the experimental values within ±10%.

4.3.4. Heat transfer rates in wall jet region ($r/d > 2.5$)

Nusselt number drops monotonically in the wall jet region almost in the similar fashion for all z/ds as shown in Figs. 7 and 8. In the wall jet region, for all z/ds covered in this study, the Nusselt number distributions overlap for a given Reynolds number. This trend is observed with results of Lytle and Webb [10] and present experimental results Fig. 9a. Decrease in the value of Nusselt numbers in this region is attributed to decrease in the velocities of fluid over the plate because of radial flow and excessive exchange of momentum of wall jet with surrounding air.

Flow regions in the wall jet can be divided into two parts *viz.* an inner layer where the effect of wall is present and an outer layer interacting with surrounding quiescent fluid. The velocity at the boundary between these two layers is the maximum local radial velocity. Poreh et al. [25], Gauntner et al. [22] and Govindan and Subba Raju [26] have shown that radial maximum velocity is inversely proportional to r^n. For $z/d \leqslant 8$, the maximum local radial velocity distribution in the wall jet region is proposed by Govindan and Subba Raju [26] and is modified to the form as given in Eq. (13)

$$\frac{U_m}{\overline{V}} = 1.545\left(\frac{z}{d}\right)^{0.122}\left(\frac{r}{d}\right)^{-1.122} \tag{13}$$

An analytical approach is discussed to interpret heat transfer coefficients in the wall jet region based on heat transfer from a flat surface of constant heat flux.

Local heat transfer to turbulent boundary layer from a flat surface of constant heat flux is given by Eq. (14), Bejan [27]

$$Nu_x = \frac{hx}{k} = 0.0308Re_x^{0.8}Pr^{0.333} \tag{14}$$

Eq. (14) can be suitably modified to express Nusselt number based on nozzle exit condition replacing x by r, a radial distance measured from stagnation point

$$Nu\left(\frac{r}{d}\right) = 0.0308\left(\frac{U_m r}{v}\right)^{0.8}Pr^{0.333} \tag{15}$$

Table 2
Enhancement factors for different z/d used in Eq. (17)

Z/d	0.5	0.75	1.0	2.0	3.0	4.0	6.0	8.0
Enhancement factor E	3.0	3.0	2.8	2.6	2.55	2.4	2.35	2.3

Substituting for U_m from Eq. (13) in Eq. (15) and rearranging the terms one obtains Eq. (16).

$$Nu = 0.0436Re_d^{0.8}Pr^{0.333}\left(\frac{z}{d}\right)^{0.0976}\left(\frac{r}{d}\right)^{-1.0976} \tag{16}$$

Appendix A details the derivation of Eq. (16) and may be used to estimate local distribution of Nusselt numbers in the wall jet region. Left side of Figs. 16 and 17 shows local distribution of Nusselt numbers in the wall jet region estimated from Eq. (16) and experimental results. It is seen that the heat transfer rates estimated from analytical approximation are lower than experimental values for all z/ds studied. Hence, Eq. (16) is modified to Eq. (17) with the enhancement factor E

$$Nu = 0.0436(E)Re^{0.8}Pr^{0.333}\left(\frac{z}{d}\right)^{0.0976}\left(\frac{r}{d}\right)^{-1.0976} \tag{17}$$

The enhancement factor E for different z/ds is listed in Table 2. The corresponding results are shown on the right side of Figs. 16 and 17. It is seen that the magnitudes of the enhancement factors decrease with increase in z/d from 3.0 to 2.3. These factors may be considered to represent heat transfer enhancements from surface of jet impingement in comparison with heat transfer from flat surface under similar flow conditions. However, the variations between analytical and experimental values are large in the initial part of wall jet for z/ds higher than 4.0.

5. Conclusions

An experimental investigation is performed to study the local distribution of heat transfer coefficients between the orthogonally impinging jet from square edged long pipe circular nozzle ($l/d = 83$) and flat plate. Reynolds number based on the nozzle exit condition is varied between 12,000 and 28,000 and jet-to-plate spacing from 0.5 to 8.0 nozzle diameters. Experiments are conducted to measure the wall static pressure distributions at different jet-to-plate spacing. A theoretical analysis is performed to derive semi-empirical correlations for the local distribution of heat transfer coefficients between impinging axisymmetric circular jet and a flat plate.

The following are the conclusions that may be drawn from this study.

- Three regions on the impingement surface are identified based on flow characteristics of impinging jet. They are stagnation region ($0 \leqslant r/d \leqslant 1.0$), transition region ($1.0 < r/d < 2.5$) and wall jet region ($r/d > 2.5$).
- Increase in Reynolds number increases the heat transfer at all the radial locations for a given z/d.

- For a given Reynolds number, Nusselt number at stagnation point increases with increase in z/d from 1.0 till around $z/d = 6.0$. This may be due to increase in near wall turbulence intensities with increase in jet-to-plate spacing. Stagnation point Nusselt numbers increase with decrease in z/d below 1.0. This may be due to flow accelerations under the jet at lower z/d. Analytical solution based on wall static pressure data in the vicinity of stagnation point confirms these trends.
- Heat transfers in the stagnation region estimated based on the simplified assumptions of an axisymmetric laminar boundary layer with favourable pressure gradient match well with present experimental results within ±6%.
- The secondary peak of local Nusselt number is observed for all z/ds below 3.0 and its location shifts towards the stagnation point with the decrease in z/d. The secondary peaks in the radial direction may occur due to flow transition in the wall jet from laminar to turbulent. These effects follow the reported results of turbulence measurements in this region.
- Semi-empirical correlation for local heat transfer rates are developed in the wall jet region based on the assumption of flow over a flat plate of constant heat flux. The solution is modified with enhancement factor (E) ranging from 3.0 to 2.3, respectively, for z/d from 0.5 to 8.0. This indicates that impinging flows can bring about enhanced heat transfer rates than similar parallel external flows.

Appendix A. Heat transfer in the wall jet region considering turbulent flow over a flat plate approach

Local Nusselt number distribution along a flat plate of constant heat flux to turbulent boundary layer is given by, Bejan [27]

$$Nu_x = 0.0308 Re_x^{0.8} Pr^{0.333} \tag{A.1}$$

where Nusselt number and Reynolds number are defined based on the distance x measured from leading edge of the flat plate. For the present case x can be replaced by r, the radial distance measured from the stagnation point. Eq. (A.1) can be put in the form

$$\frac{hr}{k} = 0.0308 \left(\frac{U_m r}{\nu}\right)^{0.8} Pr^{0.33} \tag{A.2}$$

Rearranging the terms

$$\frac{hd\left(\frac{r}{d}\right)}{k} = 0.0308 \left(\frac{U_m d\left(\frac{r}{d}\right)}{\nu}\right)^{0.8} Pr^{0.33} \tag{A.3}$$

For $z/d < 8$, Govindan and Subba Raju [26] proposed following semi-empirical relation:

$$\frac{U_m z}{\sqrt{\kappa}} = 2.229 \left(\frac{r}{z}\right)^{-1.122} \tag{A.4}$$

where κ is kinematic momentum flux of jet and is given by, Poreh et al. [25]

$$\kappa = 0.153 \pi d^2 \overline{V^2} \tag{A.5}$$

Substituting (A.5) in (A.4) one obtains

$$\frac{U_m}{\overline{V}} = 1.545 \left(\frac{z}{d}\right)^{0.122} \left(\frac{r}{d}\right)^{-1.122} \tag{A.6}$$

Substituting for U_m from (A.6) in (A.3) we get

$$Nu = 0.0436 Re^{0.8} Pr^{0.333} \left(\frac{z}{d}\right)^{0.0976} \left(\frac{r}{d}\right)^{-1.0976} \tag{A.7}$$

Nu and Re are Nusselt number and Reynolds number based on nozzle exit condition.

References

[1] J.N.B. Livingood, P. Hrycak, Impingement heat transfer from turbulent air jets to flat plates – a literature survey, NASA Technical Memorandum (NASA TM X-2778), 1970.
[2] H. Martin, Heat and mass transfer between impinging gas jets and solid surfaces, Adv. Heat Transfer 13 (1977) 1–60.
[3] K. Jambunathan, E. Lai, M.A. Moss, B.L. Button, A review of heat transfer data for single circular jet impingement, Int. J. Heat Fluid Flow 13 (1992) 106–115.
[4] R. Viskanta, Heat transfer to impinging isothermal gas and flame jets, Exp. Thermal Fluid Sci. 6 (1993) 111–134.
[5] R. Gardon, J. Cobonpue, Heat transfer between a flat plate and jets of air impinging on it, Int. Develop. Heat Transfer, ASME (1962) 454–460.
[6] R. Gardon, C. Akfirat, The role of turbulence in determining the heat transfer characteristics of impinging jets, Int. J. Heat Mass Transfer 8 (1965) 1261–1272.
[7] R. Gardon, C. Akfirat, Heat transfer characteristics of impinging two dimensional air jets, J. Heat Transfer 88 (1966) 101–108.
[8] J.W. Baughn, S. Shimizu, Heat transfer measurements from a surface with uniform heat flux and an impinging jet, J. Heat Transfer 111 (1989) 1096–1098.
[9] P. Hrycak, Heat transfer from round impinging jets to a flat plate, Int. J. Heat Mass Transfer 26 (1983) 1857–1865.
[10] D. Lytle, B.W. Webb, Air jet impingement heat transfer at low nozzle plate spacings, Int. J. Heat Mass Transfer 37 (1994) 1687–1697.
[11] D.H. Lee, J. Song, C.J. Myeong, The effect of nozzle diameter on impinging jet heat transfer and fluid flow, J. Heat Transfer 126 (2004) 554–557.
[12] A.H. Beitelmal, A.J. Shah, M.A. Saad, Analysis of an impinging two dimensional jet, J. Heat Transfer 128 (2006) 307–310.
[13] J.H. Lienhard, Heat transfer by impingement of circular free-surface liquid jets, in: 18th National and 7th ISHMT – ASME Heat and Mass Transfer Conference, January 4–6, 2006.
[14] S.V. Garimella, B. Nenaydykh, Nozzle-geometry effects in liquid jet impingement heat transfer, Int. J. Heat Mass Transfer 39 (1996) 2915–2923.
[15] J. Lee, S.-J. Lee, The effect of nozzle configuration on stagnation region heat transfer enhancement of axisymmetric jet impingement, Int. J. Heat Mass Transfer 43 (2000) 3497–3509.
[16] L.A. Brignoni, S.V. Garimella, Effects of nozzle inlet chamfering on pressure drop and heat transfer in confined air jet impingement, Int. J. Heat Mass Transfer 43 (2000) 1133–1139.
[17] N. Zuckerman, N. Lior, Impingement heat transfer: correlations and numerical modeling, J. Heat Transfer 127 (2005) 544–552.
[18] R.J. Moffat, Describing the uncertainties in experimental results, Exp. Thermal Fluid Sci. 1 (1988) 3–17.
[19] N. Gao, H. Sun, D. Ewing, Heat transfer to impinging round jets with triangular tabs, Int. J. Heat Mass Transfer 46 (2003) 2557–2569.
[20] D. Cooper, D.C. Jackson, B.E. Launder, G.X. Liao, Impingement jet studies for turbulence model assessment – I. Flow-field experiments, Int. J. Heat Mass Transfer 36 (1993) 2675–2684.

[21] L.C. Burmister, Convective Heat Transfer, second ed., John Wiley and Sons, Inc., 1993.
[22] J.W. Gauntner, J.N.B. Livingood, P. Hrycak, Survey of literature on flow characteristics of a single turbulent jet impinging on a flat plate, NASA Technical Note (NASA TN D-5652), 1970.
[23] P.M. Brdlik, V.K. Savin, Heat transfer in the vicinity of stagnation point in an axisymmetric jet flowing flat surfaces normal to the flow, J. Eng Phys. 10 (1966) 423–428.
[24] K. Knowles, M. Myszko, Turbulence measurements in radial wall-jets, Exp. Thermal Fluid Sci. 17 (1998) 71–78.
[25] M. Poreh, Y.G. Tsuei, J.E. Cermak, Investigation of a turbulent radial wall jet, J. Appl. Mech. 34 (1967) 457–463.
[26] A.P. Govindan, K. Subba Raju, Hydrodynamics of a radial wall jet, J. Appl. Mech. 41 (1974) 518–519.
[27] A. Bejan, Convection Heat Transfer, third ed., John Wiley and Sons, 2004, p. 357.